Topological flat bands in optical checkerboardlike lattices

Tomi Paananen and Thomas Dahm
Universität Bielefeld, Fakultät für Physik, Postfach 100131, D-33501 Bielefeld, Germany
(Received 21 August 2014; published 4 March 2015)

We present comparatively simple two-dimensional and three-dimensional checkerboardlike optical lattices possessing nontrivial topological properties accompanied by topological surface states. By simple tuning of the parameters, these lattices can have a topological insulating phase, a topological semimetallic phase, or a trivial insulating phase. This allows the study of different topological phase transitions within a single cold-atom system. In the topologically nontrivial phases, flat bands appear at the surfaces of the system. These surface states possess short localization lengths such that they are observable even in systems with small lattice dimensions.

DOI: 10.1103/PhysRevA.91.033604 PACS number(s): 67.85.−d, 37.10.Jk, 05.30.Fk, 03.65.Vf

I. INTRODUCTION

The theoretical prediction [1,2] and experimental discovery of topological insulators [3,4] has spurred the interest in nontrivial topological phases. The common property of these systems is the fact that surface states are protected by topological quantum numbers, making them particularly stable against different kinds of perturbations [5]. In particular, topological semimetals such as Dirac semimetals and Weyl semimetals and their unusual surface states have been studied recently in condensed-matter systems [6–11].

Optical lattices with cold atoms are perfect tools to simulate condensed-matter problems. Using optical lattices, one can modify lattice depths and lattice structures [12–15]. That is why almost any condensed-matter system can be simulated using optical lattices. Interactions between cold atoms can also be tuned via the Feshbach resonance [16,17]. Several proposals have been made to realize topologically nontrivial states in cold-atom systems [18–25] and, recently, the first experimental realizations in optical lattices have been demonstrated [26–28].

In the present work, we make a specific proposal as to how topological surface flat bands can be realized using comparatively simple optical lattices. Flat band states are particularly interesting because the group velocity vanishes, and highly localized states can be formed. Also, the effect of interactions becomes particularly important in flat bands, allowing new states of quantum matter [29–31] or interaction-driven phase transitions, for example a ferromagnetic state in graphene nanoribbons [32] or surface superconductivity with high critical temperature [33,34]. A distinction has to be made between bulk flat bands that appear through the whole system in certain types of lattices [29–31,35–38] and surface flat bands that are guaranteed to exist at the surface of a topologically nontrivial system as a consequence of bulk-boundary correspondence [39–42]. The present work is concerned with the latter case. Such kind of topological surface flat bands has been found previously in other condensed-matter systems such as graphene, superfluid ^{3}He, or unconventional superconductors [43–59], and may also appear in topological insulators with a time-reversal breaking ferromagnetic exchange field [41,42,60]. The appearance of flat bands in d-wave superconductors as surface Andreev bound states has been studied intensively in the past, both theoretically and experimentally [39,51–53,61–73]. Using optical lattices with ultracold atoms, such surface flat bands and, in particular, the influence of interactions on them could be studied in a very controlled way. Experimentally, surface states in cold-atom systems can be detected by Bragg spectroscopy [19,21] or a combination of Ramsey interference and Bloch oscillations [74].

In this work, we will present a two-dimensional (2D) and a three-dimensional (3D) optical lattice model, possessing one-dimensional and two-dimensional surface flat bands, respectively. We will give simple analytical criteria for the existence and location of these flat bands. Using two independent means—exact numerical diagonalization and an analytical method—we demonstrate that the system can be tuned from a topological insulating phase via a topological semimetallic phase to a trivial insulating phase by tuning the intensity of the lasers creating the lattice. This allows the study of various interesting topological phase transitions within a single model. We also show that in the 3D case, the flat bands are always two dimensional, and the flat bands can be doubly degenerate under some circumstances. Flat bands can appear both for an insulating as well as a semimetallic bulk phase. The appearance of the flat bands can be understood in terms of a classification recently proposed by Matsuura *et al.* [40] using a topological invariant in the presence of a chiral symmetry.

II. MODELS

A. Two-dimensional model

Our model is a tight-binding checkerboard model with different forward and backward hoppings. The Hamiltonian can be written as

$$\begin{aligned}\hat{H}_{2D} = \sum_{m,n}(&-J_{1,x}\hat{a}^\dagger_{1,m,n}\hat{b}_{1,m,n} - J_{2,x}\hat{a}^\dagger_{1,m,n}\hat{b}_{1,m-1,n}\\ &-J_{1,x}\hat{a}^\dagger_{2,m,n}\hat{b}_{2,m+1,n} - J_{2,x}\hat{a}^\dagger_{2,m,n}\hat{b}_{2,m,n}\\ &-J_{1,y}\hat{a}^\dagger_{1,m,n}\hat{b}_{2,m,n} - J_{2,y}\hat{a}^\dagger_{1,m,n}\hat{b}_{2,m,n-1}\\ &-J_{1,y}\hat{a}^\dagger_{2,m,n}\hat{b}_{1,m,n+1} - J_{2,y}\hat{a}^\dagger_{2,m,n}\hat{b}_{1,m,n} + \text{H.c.}),\end{aligned} \quad (1)$$

where m and n are the unit cell indices, and $\hat{a}$ and $\hat{b}$ are annihilation operators for different sublattice sites. This Hamiltonian is essentially a two-dimensional generalization of the dimerized optical lattice that has been studied in Ref. [26]. It consists of four sublattice sites per unit cell, as shown in Fig. 1. If the periodicity of the lattice is d, then the lattice spacing of the sublattice is $d/2$. We can assume without loss

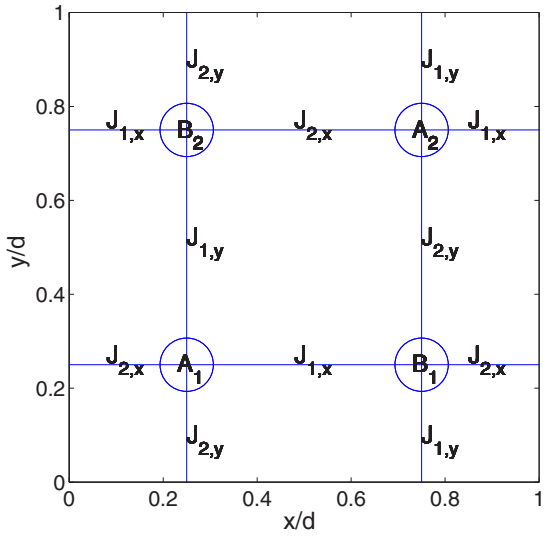

FIG. 1. (Color online) Schematic figure of the sublattice structure and the corresponding hopping strengths.

of generality that $J_{1,\alpha} \geqslant J_{2,\alpha}$ (if this is not the case, we can always relabel the hopping strengths and the sublattice sites). In Appendix A, we discuss how such an optical lattice can be created by a certain laser arrangement. Recently, there has been intensive experimental effort to create either spin-orbit coupling [24] or non-Abelian gauge potentials [75,76] in cold-atom systems in a desire to simulate topological insulators. We note that neither spin-orbit coupling nor a non-Abelian gauge potential is needed to create the present lattice. Nevertheless, topological surface states appear for certain parameter ranges, as shown below.

If one takes the Fourier transform of the Hamiltonian, it can be written as

$$H_{2D} = \sum_{\mathbf{k}} \hat{\Psi}_{\mathbf{k}}^{\dagger} \begin{pmatrix} 0 & 0 & f_x^*(k_x) & f_y^*(k_y) \\ 0 & 0 & f_y^*(k_y) & f_x^*(k_x) \\ f_x(k_x) & f_y(k_y) & 0 & 0 \\ f_y(k_y) & f_x(k_x) & 0 & 0 \end{pmatrix} \hat{\Psi}_{\mathbf{k}}, \tag{2}$$

where $\mathbf{k} = (k_x, k_y)$,

$$\hat{\Psi}_{\mathbf{k}} = (\hat{a}_{1,\mathbf{k}}, \hat{a}_{2,\mathbf{k}}, \hat{b}_{1,\mathbf{k}}, \hat{b}_{2,\mathbf{k}})^T,$$

and

$$f_\alpha(k_\alpha) = -J_{1,\alpha} e^{ik_\alpha d/2} - J_{2,\alpha} e^{-ik_\alpha d/2}. \tag{3}$$

The Hamiltonian possesses particle-hole symmetry if the system is half filled with two fermions per unit cell. Also, time-reversal symmetry, parity symmetry, and, most importantly, a chiral symmetry

$$S = \begin{pmatrix} 1 & 0 & 0 & 0 \\ 0 & 1 & 0 & 0 \\ 0 & 0 & -1 & 0 \\ 0 & 0 & 0 & -1 \end{pmatrix} \tag{4}$$

are respected, i.e., H_{2D} and S anticommute. As has been discussed in Refs. [78,79], the chiral symmetry S is essential for the existence of edge flat bands. Note that the phases of f_x and f_y cannot be transformed away by a gauge transformation as they correspond to a Berry phase [77].

The single-particle Hamiltonian has an off-diagonal block form, thus the methods from Refs. [40,80] can be used to treat the Hamiltonian. In our case, the block is given by

$$D_{2D}(\mathbf{k}) = \begin{pmatrix} f_x(k_x) & f_y(k_y) \\ f_y(k_y) & f_x(k_x) \end{pmatrix}. \tag{5}$$

For a boundary perpendicular to the x direction, the existence of edge flat bands is connected to the value of the following winding number [40,80]:

$$w(k_y) = \frac{1}{2\pi} \mathrm{Im} \left[\int_{-\pi}^{\pi} dk_x \, \frac{\partial_{k_x} \mathrm{Det}[D_{2D}(\mathbf{k})]}{\mathrm{Det}[D_{2D}(\mathbf{k})]} \right]. \tag{6}$$

Here we have set $d = 1$. We can define the path $\gamma(k_x) = \mathrm{Det}[D_{2D}(\mathbf{k})] = f_x(k_x)^2 - f_y(k_y)^2$ in the complex plane. Then, this integral can be written as a path integral as follows:

$$w(k_y) = \frac{1}{2\pi i} \oint_{\gamma} \frac{dz}{z}. \tag{7}$$

This shows that the winding number $w(k_y)$ is always an integer. If it is equal to zero, we do not have a flat band at the surface, otherwise we do. However, this formula is not very useful to determine the values of k_y for which a flat band exists. Instead, setting $z = e^{ik_x d}$, integral (6) can be mapped to a path integral over the unit circle, and the integrand is then given by

$$\begin{aligned} f_{2D}(z) &= \frac{J_{1,x}^2 z^2 - J_{2,x}^2}{z[(J_{1,x} z + J_{2,x})^2 - z f_y(k_y)^2]} \\ &= \frac{-1}{z} + \frac{1}{z - w_+} + \frac{1}{z - w_-}, \end{aligned} \tag{8}$$

where

$$w_\pm = \left[\frac{f_y(k_y) \pm \sqrt{f_y(k_y)^2 - 4 J_{1,x} J_{2,x}}}{2 J_{1,x}} \right]^2. \tag{9}$$

Let us assume first that $J_{1,x} > J_{2,x}$. The absolute values of $w_\pm$ determine whether or not we have a flat band. It is easy to prove that one of the absolute values is always smaller than $J_{2,x}/J_{1,x} < 1$. Thus, if both are smaller than 1, we have a flat band; if not, we do not have a flat band. It turns out that

$$\begin{aligned} &\max(|w_+|, |w_-|) \leqslant \left\{ \frac{(J_{1,x} - J_{2,x})|V_{k_y}| + \sqrt{[(J_{1,x} - J_{2,x})|V_{k_y}|]^2 + 4 J_{1,x} J_{2,x}}}{2 J_{1,x}} \right\}^2 \quad \text{if} \quad |V_{k_y}| < 1 \\ &\max(|w_+|, |w_-|) = 1 \quad \text{if} \quad |V_{k_y}| = 1 \\ &\max(|w_+|, |w_-|) \geqslant \left\{ \frac{(J_{1,x} - J_{2,x})|V_{k_y}| + \sqrt{[(J_{1,x} - J_{2,x})|V_{k_y}|]^2 + 4 J_{1,x} J_{2,x}}}{2 J_{1,x}} \right\}^2 \quad \text{if} \quad |V_{k_y}| > 1, \end{aligned} \tag{10}$$

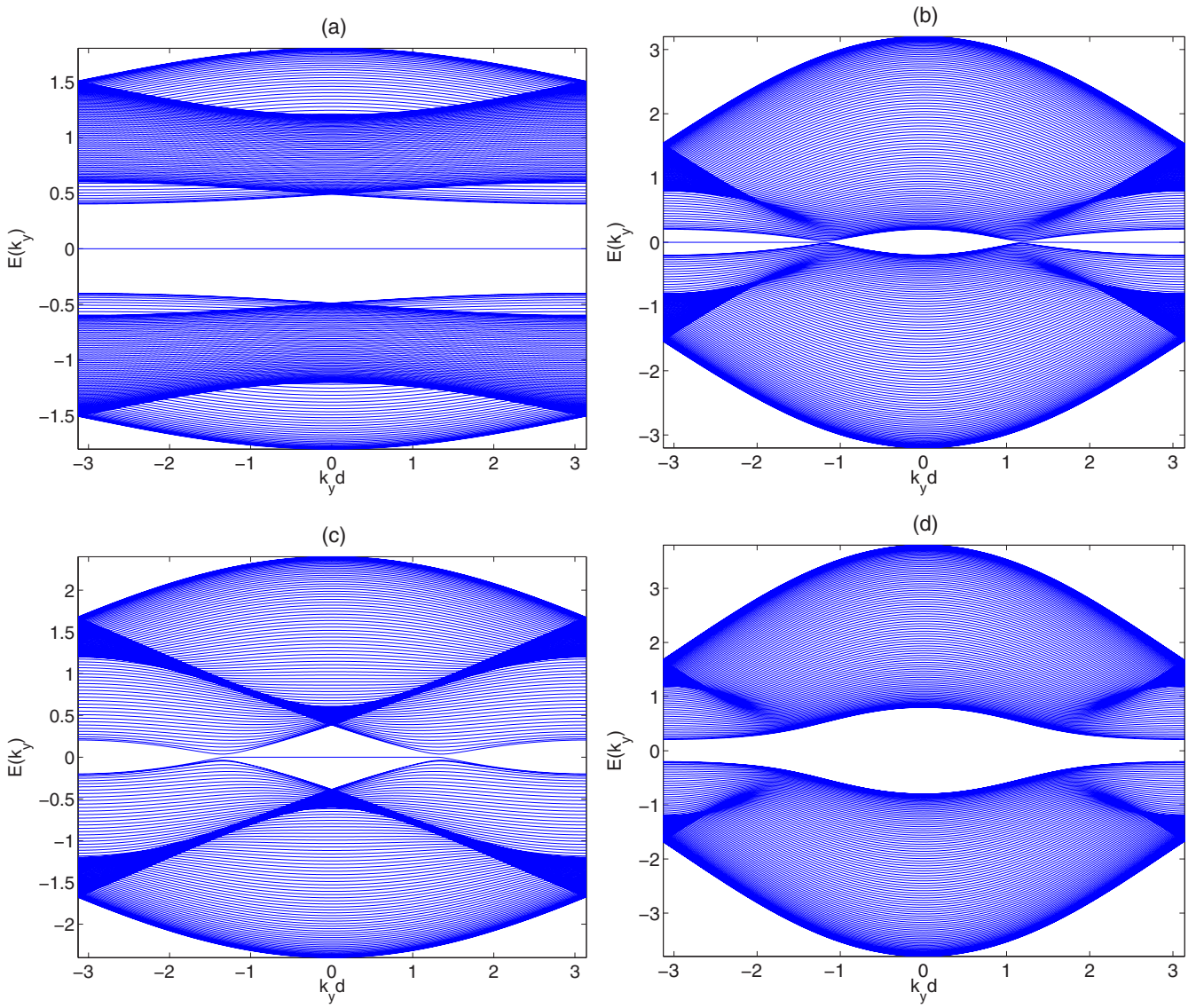

FIG. 2. (Color online) Numerical 2D dispersions of bulk and edge states for $J_{1,x} = 1.0$ and $J_{2,x} = 0.5$ with different values of $J_{1,y}$ and $J_{2,y}$. (a) $J_{1,y} = 0.2$ and $J_{2,y} = 0.1$, (b) $J_{1,y} = 1.0$ and $J_{2,y} = 0.7$, (c) $J_{1,y} = 0.8$ and $J_{2,y} = 0.1$, and (d) $J_{1,y} = 1.5$ and $J_{2,y} = 0.8$.

where

$$|V_{k_y}|^2 = \left(\frac{J_{1,y} + J_{2,y}}{J_{1,x} + J_{2,x}}\right)^2 \cos^2(k_y/2) + \left(\frac{J_{1,y} - J_{2,y}}{J_{1,x} - J_{2,x}}\right)^2 \sin^2(k_y/2) = a_y^2 \cos^2(k_y/2) + b_y^2 \sin^2(k_y/2),$$

with $a_y = |\frac{J_{1,y}+J_{2,y}}{J_{1,x}+J_{2,x}}|$ and $b_y = |\frac{J_{1,y}-J_{2,y}}{J_{1,x}-J_{2,x}}|$. Equation (10) shows that $\max(|w_+|,|w_-|) < 1$, if $|V_{k_y}| < 1$, and $\max(|w_+|,|w_-|)>1$, if $|V_{k_y}| > 1$. From this, we can deduce that we have a flat band only if $|V_{k_y}| < 1$. From Eq. (10), we can deduce the following: If both $a_y < 1$ and $b_y<1$, then we have an edge flat band for all k_y, and the bulk is an insulator. Thus, in this case, the flat bands are isolated. If $a_y \geqslant 1$ and $b_y < 1$, we have a flat band for

$$|k_y| > 2 \arccos\left(\sqrt{\frac{1 - b_y^2}{a_y^2 - b_y^2}}\right),$$

and the bulk is a topological semimetal. If $a_y < 1$ and $b_y \geqslant 1$, we have a flat band for

$$|k_y| < 2 \arccos\left(\sqrt{\frac{b_y^2 - 1}{b_y^2 - a_y^2}}\right),$$

with the bulk being a semimetal, too. If both $a_y \geqslant 1$ and $b_y \geqslant 1$, then we have no flat bands. If $a_y > 1$ and $b_y > 1$, then we have an insulating bulk without edge states, i.e., a topologically trivial insulator. Thus, by tuning the optical lattice potential via the parameters a_y and b_y, it becomes possible to drive the system into different topological phases.

In order to confirm these analytical results based on the winding number given in Ref. [40], we numerically determined

all eigenvalues by exact diagonalization of Hamiltonian (1) on a finite lattice. We use periodical boundary conditions in the y direction and open boundary conditions in the x direction. Results of the numerical exact diagonalization on a 200×200 lattice are shown in Fig. 2, which presents the energy spectra as a function of momentum k_y parallel to the surface for $J_{1,x} = 1.0$ and $J_{2,x} = 0.5$ with different values of $J_{1,y}$ and $J_{2,y}$. The values we have chosen correspond to the four different topological phases mentioned above. Figure 2(a) demonstrates that for $a_y < 1$ and $b_y < 1$, there exists an edge flat band for all momenta k_y, and the bulk is an insulator. Figure 2(b) demonstrates that for $a_y > 1$ and $b_y < 1$, there exists an edge flat band for a finite range of momenta with

$$|k_y| > 2 \arccos\left(\sqrt{\frac{1-b_y^2}{a_y^2-b_y^2}}\right).$$

Figure 2(c) demonstrates that for $a_y < 1$ and $b_y > 1$, there exists an edge flat band for a finite range of momenta with

$$|k_y| < 2 \arccos\left(\sqrt{\frac{b_y^2-1}{b_y^2-a_y^2}}\right).$$

Finally, Fig. 2(d) shows that for $a_y > 1$ and $b_y > 1$, there is no flat band and the bulk is insulating, corresponding to a trivial insulator.

Figure 3 demonstrates that the wave functions of the flat band states are indeed localized at the edge of the system. The figure shows the occupation probabilities $|\rho(n)|^2$ as a function of unit cell index n of selected edge [Figs. 3(a)–3(c)] and bulk [Fig. 3(d)] states for $J_{1,x} = 1.0$ and $J_{1,x} = 0.5$ with different values of $J_{1,y}$ and $J_{2,y}$. We see from Figs. 3(a)–3(c) that the edge states are well localized on the boundary within the first 5 to 10 lattice sites. Thus the flat bands should be visible even for small lattice size. The localization becomes better if $|J_{1,x} - J_{2,x}|/(J_{1,x} + J_{2,x})$ increases.

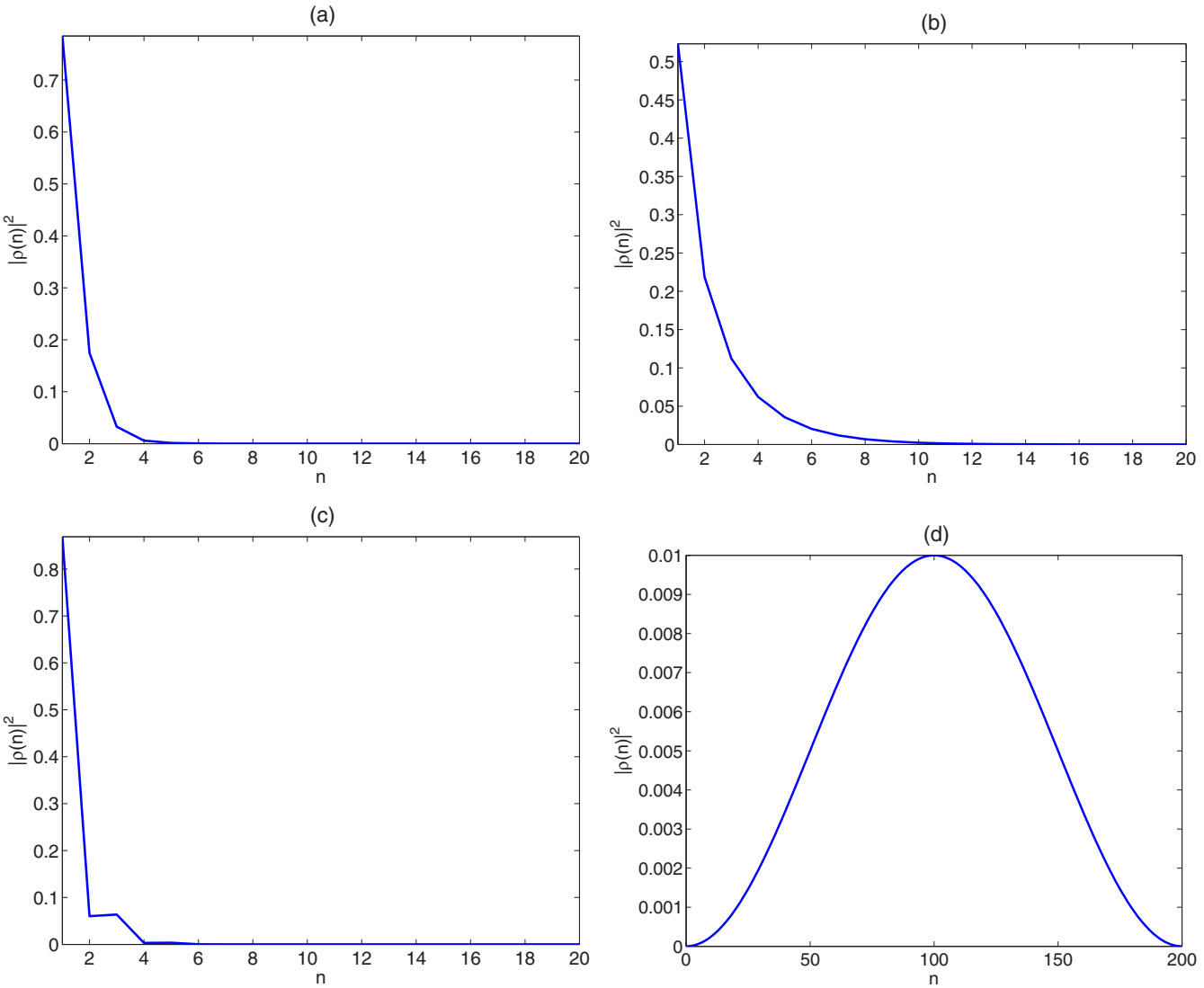

FIG. 3. (Color online) Occupation probabilities $|\rho(n)|^2$ as a function of unit cell index n of selected (a)–(c) edge and (d) bulk states for $J_{1,x} = 1.0$ and $J_{2,x} = 0.5$ with different values of $J_{1,y}$ and $J_{2,y}$. (a) $J_{1,y} = 0.2$, $J_{2,y} = 0.1$, and $k_y = 0$, (b) $J_{1,y} = 1.0$, $J_{2,y} = 0.7$, and $k_y = \pi$, (c) $J_{1,y} = 0.8$, $J_{2,y} = 0.1$, and $k_y = 0$, and (d) $J_{1,y} = 1.5$, $J_{2,y} = 0.8$, and $k_y = 0$.

If $J_{2,x} = J_{1,x}$, then we have no flat bands. In this case, the analytical method described above cannot always be used because the integral (6) does not converge in this case. However, in this case, we can deduce that if $k_y \neq 0$ and $J_{y,1} \neq J_{y,2}$, then $\max(|w_+|,|w_-|) > 1$ and $\min(|w_+|,|w_-|) < 1$. Thus no flat bands appear. If $k_y = 0$ or $J_{y,1} = J_{y,2}$, then the integral (6) does not converge because of poles on the integration path. In this case, the projection of the Fermi surface onto the boundary forms a continuum with the bulk states, and thus we have no edge flat bands.

B. Three-dimensional model

The three-dimensional case is a direct generalization of the 2D case. The Hamiltonian can be written as

$$\begin{aligned}\hat{H}_{3D} = \sum_{m,n,i}(&-J_{1,x}\hat{a}^\dagger_{1,m,n,i}\hat{b}_{1,m,n,i} - J_{2,x}\hat{a}^\dagger_{1,m,n,i}\hat{b}_{1,m-1,n,i} - J_{1,x}\hat{a}^\dagger_{2,m,n,i}\hat{b}_{2,m+1,n,i} - J_{2,x}\hat{a}^\dagger_{2,m,n,i}\hat{b}_{2,m,n,i}\\ &- J_{1,x}\hat{a}^\dagger_{3,m,n,i}\hat{b}_{3,m+1,n,i} - J_{2,x}\hat{a}^\dagger_{3,m,n,i}\hat{b}_{3,m,n,i} - J_{1,x}\hat{a}^\dagger_{4,m,n,i}\hat{b}_{4,m,n,i} - J_{2,x}\hat{a}^\dagger_{4,m,n,i}\hat{b}_{4,m-1,n,i}\\ &- J_{1,y}\hat{a}^\dagger_{1,m,n,i}\hat{b}_{2,m,n,i} - J_{2,y}\hat{a}^\dagger_{1,m,n,i}\hat{b}_{2,m,n-1,i} - J_{1,y}\hat{a}^\dagger_{2,m,n,i}\hat{b}_{1,m,n+1} - J_{2,y}\hat{a}^\dagger_{2,m,n,i}\hat{b}_{1,m,n,i}\\ &- J_{1,y}\hat{a}^\dagger_{3,m,n,i}\hat{b}_{4,m,n+1,i} - J_{2,y}\hat{a}^\dagger_{3,m,n,i}\hat{b}_{4,m,n,i} - J_{1,y}\hat{a}^\dagger_{4,m,n,i}\hat{b}_{3,m,n} - J_{2,y}\hat{a}^\dagger_{4,m,n,i}\hat{b}_{3,m,n-1,i}\\ &- J_{1,z}\hat{a}^\dagger_{1,m,n,i}\hat{b}_{3,m,n,i} - J_{2,z}\hat{a}^\dagger_{1,m,n,i}\hat{b}_{3,m,n,i-1} - J_{1,z}\hat{a}^\dagger_{2,m,n,i}\hat{b}_{4,m,n,i} - J_{2,z}\hat{a}^\dagger_{2,m,n,i}\hat{b}_{4,m,n,i-1}\\ &- J_{1,z}\hat{a}^\dagger_{3,m,n,i}\hat{b}_{2,m,n,i+1} - J_{2,z}\hat{a}^\dagger_{3,m,n,i}\hat{b}_{2,m,n,i} - J_{1,z}\hat{a}^\dagger_{4,m,n,i}\hat{b}_{1,m,n,i+1} - J_{2,z}\hat{a}^\dagger_{4,m,n,i}\hat{b}_{1,m,n,i} + \text{H.c.}),\end{aligned} \tag{11}$$

where m, n, and i are the unit cell indices, and $\hat{a}$ and $\hat{b}$ are annihilation operators. This Hamiltonian consists of eight sublattice sites per unit cell.

If one takes a Fourier transform of the Hamiltonian, the Hamiltonian can be written as

$$H_{3D} = \sum_{\mathbf{k}} \hat{\Psi}^\dagger_{\mathbf{k}} \begin{pmatrix} 0 & 0 & 0 & 0 & f^*_x(k_x) & f^*_y(k_y) & f^*_z(k_z) & 0 \\ 0 & 0 & 0 & 0 & f^*_y(k_y) & f^*_x(k_x) & 0 & f^*_z(k_z) \\ 0 & 0 & 0 & 0 & f^*_z(k_z) & 0 & f^*_x(k_x) & f^*_y(k_y) \\ 0 & 0 & 0 & 0 & 0 & f^*_z(k_z) & f^*_y(k_y) & f^*_x(k_x) \\ f_x(k_x) & f_y(k_y) & f_z(k_z) & 0 & 0 & 0 & 0 & 0 \\ f_y(k_y) & f_x(k_x) & 0 & f_z(k_z) & 0 & 0 & 0 & 0 \\ f_z(k_z) & 0 & f_x(k_x) & f_y(k_y) & 0 & 0 & 0 & 0 \\ 0 & f_z(k_z) & f_y(k_y) & f_x(k_x) & 0 & 0 & 0 & 0 \end{pmatrix} \hat{\Psi}_{\mathbf{k}}, \tag{12}$$

where $\mathbf{k} = (k_x,k_y,k_z)$,

$$\hat{\Psi}_{\mathbf{k}} = (\hat{a}_{1,\mathbf{k}},\hat{a}_{2,\mathbf{k}},\hat{a}_{3,\mathbf{k}},\hat{a}_{4,\mathbf{k}},\hat{b}_{1,\mathbf{k}},\hat{b}_{2,\mathbf{k}},\hat{b}_{3,\mathbf{k}},\hat{b}_{4,\mathbf{k}})^T,$$

and

$$f_\alpha(k_\alpha) = -J_{1,\alpha}e^{ik_\alpha d/2} - J_{2,\alpha}e^{-ik_\alpha d/2}. \tag{13}$$

As in the 2D case, this Hamiltonian has a particle-hole symmetry, time-reversal symmetry, and a parity symmetry. Most importantly, the Hamiltonian exhibits a chiral symmetry, again allowing for the existence of topological edge flat bands [78,79]. Also this Hamiltonian has an off-diagonal block form, thus the methods from Refs. [40,80] can be used to treat the Hamiltonian again. In the present case, the block is given by

$$D_{3D}(\mathbf{k}) = \begin{pmatrix} f_x(k_x) & f_y(k_y) & f_z(k_z) & 0 \\ f_y(k_y) & f_x(k_x) & 0 & f_z(k_z) \\ f_z(k_z) & 0 & f_x(k_x) & f_y(k_y) \\ 0 & f_z(k_z) & f_y(k_y) & f_x(k_x) \end{pmatrix}. \tag{14}$$

If we consider a boundary perpendicular to the x direction, the existence of edge flat bands is connected to the value of the following winding number [40,80]:

$$w(k_y,k_z) = \frac{1}{2\pi}\mathrm{Im}\left\{\int_{-\pi}^{\pi} dk_x \frac{\partial_{k_x}\mathrm{Det}[D_{3D}(\mathbf{k})]}{\mathrm{Det}[D_{3D}(\mathbf{k})]}\right\}. \tag{15}$$

Again, this integral can be mapped to a path integral over the unit circle, and the integrand is then given by

$$f_{3D}(z) = \frac{p_1(z)}{z p_2(z)}, \tag{16}$$

where

$$\begin{aligned} p_1(z) &= 2J^4_{1,x}z^4 + 4J^3_{1,x}J_{2,x}z^3 - 4J^3_{2,x}J_{1,x}z - 2J^4_{2,x}\\ &\quad - 2\left(J^2_{1,x}z^3 - J^2_{2,x}z\right)[f_y(k_y)^2 + f_z(k_z)^2],\\ p_2(z) &= (J_{1,x}z + J_{2,x})^4\\ &\quad - 2z\{(J_{1,x}z + J_{2,x})^2[f_y(k_y)^2 + f_z(k_z)^2]\}\\ &\quad + z^2[f_y(k_y)^4 + f_z(k_z)^4 - 2f_y(k_y)^2 f_z(k_z)^2]. \end{aligned}$$

Integrand (16) can be simplified as

$$f_{3D}(z) = \frac{-2}{z} + \frac{1}{z - w^+_+} + \frac{1}{z - w^+_-} + \frac{1}{z - w^-_+} + \frac{1}{z - w^-_-}, \tag{17}$$

where

$$w_{\pm}^{+} = \left\{ \frac{[f_y(k_y) + f_z(k_z)] \pm \sqrt{[f_y(k_y) + f_z(k_z)]^2 - 4J_{1,x}J_{2,x}}}{2J_{1,x}} \right\}^2,$$
$$w_{\pm}^{-} = \left\{ \frac{[f_y(k_y) - f_z(k_z)] \pm \sqrt{[f_y(k_y) - f_z(k_z)]^2 - 4J_{1,x}J_{2,x}}}{2J_{1,x}} \right\}^2. \tag{18}$$

Thus the integral can assume the values $-2, -1, 0, 1, 2$. If the value is 0, then there are no flat bands, but otherwise there are. If the value equals 2 (or -2), we find two degenerate flat bands.

Let us assume $J_{1,x} > J_{2,x}$. Now, $\min(|w_+^+|, |w_-^+|) \leqslant J_{2,x}/J_{1,x} < 1$ and $\min(|w_+^-|, |w_-^-|) \leqslant J_{2,x}/J_{1,x} < 1$. Thus we always have at least two poles within the unit disk. Thus the value of the integral depends on the values of $\max(|w_+^+|, |w_-^+|)$ and $\max(|w_+^-|, |w_-^-|)$. It turns out that

$$\max(|w_+^{\pm}|, |w_-^{\pm}|) \leqslant \left\{ \frac{(J_{1,x} - J_{2,x})\left|V_{k_y,k_z}^{\pm}\right| + \sqrt{\left[(J_{1,x} - J_{2,x})\left|V_{k_y,k_z}^{\pm}\right|\right]^2 + 4J_{1,x}J_{2,x}}}{2J_{1,x}} \right\}^2 \quad \text{if} \quad \left|V_{k_y,k_z}^{\pm}\right| < 1$$
$$\max(|w_+^{\pm}|, |w_-^{\pm}|) = 1 \quad \text{if} \quad \left|V_{k_y,k_z}^{\pm}\right| = 1 \tag{19}$$
$$\max(|w_+^{\pm}|, |w_-^{\pm}|) \geqslant \left\{ \frac{(J_{1,x} - J_{2,x})\left|V_{k_y,k_z}^{\pm}\right| + \sqrt{\left[(J_{1,x} - J_{2,x})\left|V_{k_y,k_z}^{\pm}\right|\right]^2 + 4J_{1,x}J_{2,x}}}{2J_{1,x}} \right\}^2 \quad \text{if} \quad \left|V_{k_y,k_z}^{\pm}\right| > 1,$$

where

$$\left|V_{k_y,k_z}^{\pm}\right|^2 = \left[\frac{J_{1,y} + J_{2,y}}{J_{1,x} + J_{2,x}} \cos(k_y/2) \pm \frac{J_{1,z} + J_{2,z}}{J_{1,x} + J_{2,x}} \cos(k_z/2)\right]^2 + \left[\frac{J_{1,y} - J_{2,y}}{J_{1,x} - J_{2,x}} \sin(k_y/2) \pm \frac{J_{1,z} - J_{2,z}}{J_{1,x} - J_{2,x}} \sin(k_z/2)\right]^2$$
$$= [a_y \cos(k_y/2) \pm a_z \cos(k_z/2)]^2 + [b_y \sin(k_y/2) \pm b_z \sin(k_z/2)]^2.$$

If $|V_{k_y,k_z}^{\pm}| < 1$, then $\max(|w_+^{\pm}|, |w_-^{\pm}|) < 1$, and if $|V_{k_y,k_z}^{\pm}| > 1$, then $\max(|w_+^{\pm}|, |w_-^{\pm}|) > 1$. If both $\max(|w_+^{\pm}|, |w_-^{\pm}|)$ are smaller than 1, we find two flat bands; if only one is smaller than 1, we find a single flat band; and if both are larger than 1, we find no flat bands.

The location (in the projected momentum space, i.e., in the $k_y k_z$ plane) of the flat bands depends on the parameters a_y, a_z, b_y, b_z. Without loss of generality, we can assume that all of these parameters are non-negative. In this case, $\sup_{k_y,k_z} |V_{k_y,k_z}^{+}| \geqslant \sup_{k_y,k_z} |V_{k_y,k_z}^{-}|$ and $\inf_{k_y,k_z} |V_{k_y,k_z}^{+}| \geqslant \inf_{k_y,k_z} |V_{k_y,k_z}^{-}|$. The values of $\sup_{k_y,k_z} |V_{k_y,k_z}^{+}|$, $\sup_{k_y,k_z} |V_{k_y,k_z}^{-}|$, $\inf_{k_y,k_z} |V_{k_y,k_z}^{+}|$, and $\inf_{k_y,k_z} |V_{k_y,k_z}^{-}|$ can be found in Appendix B.

We have several different phase possibilities: (i) If $\sup_{k_y,k_z} |V_{k_y,k_z}^{+}| < 1$, then the bulk is an insulator, and we find two isolated flat bands for every $\tilde{\mathbf{k}} = (k_y, k_z)$. (ii) If $\sup_{k_y,k_z} |V_{k_y,k_z}^{-}| < 1$, $\sup_{k_y,k_z} |V_{k_y,k_z}^{+}| \geqslant 1$, and $\inf_{k_y,k_z} |V_{k_y,k_z}^{+}| < 1$, then the bulk is a semimetal, and we find a flat band for all $\tilde{\mathbf{k}}$. For some $\tilde{\mathbf{k}}$, there are two flat bands, and one flat band for the rest. (iii) If $\inf_{k_y,k_z} |V_{k_y,k_z}^{+}| < 1$ and $\sup_{k_y,k_z} |V_{k_y,k_z}^{-}| \geqslant 1$, then the bulk is a semimetal. Flat bands can be found only in some part of the projected k space. (iv) If $\inf_{k_y,k_z} |V_{k_y,k_z}^{+}| > 1$, $\inf_{k_y,k_z} |V_{k_y,k_z}^{-}| < 1$, and $\sup_{k_y,k_z} |V_{k_y,k_z}^{-}| \geqslant 1$, then the bulk is a semimetal, and we have a nondegenerate flat band in some part of the projected momentum space. (v) If $\inf_{k_y,k_z} |V_{k_y,k_z}^{-}| > 1$, then the bulk is an insulator, and we find no flat bands.

One could move from one phase to another by tuning the laser intensity.

Figure 4 shows some examples of 2D flat bands in the surface Brillouin zone for the different phases. In Fig. 4(a), we show phase I with $J_{1,y} = J_{1,z} = 0.2$ and $J_{2,y} = J_{2,z} = 0.1$. Here we see that the twofold degenerate flat band totally fills the projected momentum space. Figure 4(b) shows phase II with $J_{1,y} = 0.6$, $J_{1,z} = 0.4$, and $J_{2,y} = J_{2,z} = 0.2$, where the twofold degenerate flat band fills the projected momentum space only partially, and the rest of the momentum space (near the origin) is filled by a nondegenerate flat band. Phase III with $J_{1,y} = J_{1,z} = 1.0$, $J_{2,y} = 0.8$, and $J_{2,z} = 0.6$ is shown in Fig. 4(c). In this case, we see that only a part of the projected momentum space is occupied by the flat bands (degenerate and nondegenerate). In Fig. 4(d), we show phase IV with $J_{1,y} = 2.0$, $J_{1,z} = 1.2$, $J_{2,y} = 0.3$, and $J_{2,z} = 0.4$. Here we see that only a nondegenerate flat band partially fills the projected momentum space. Throughout Fig. 4, we have set $J_{1,x} = 1.0$ and $J_{1,x} = 0.2$.

If $J_{1,x} = J_{2,x}$, there are no flat bands. The reasons are the same as in the 2D case. If one looks at all three possible boundaries (perpendicular to the x, y, or z direction), the only situation when one cannot find any flat bands is the case where $J_{1,x} = J_{2,x}$, $J_{1,y} = J_{2,y}$, and $J_{1,z} = J_{2,z}$. In this case, the bulk is a metal (a standard cubic lattice). Thus if the bulk is an insulator or a semimetal, one can always find flat bands at least at one of the boundaries.

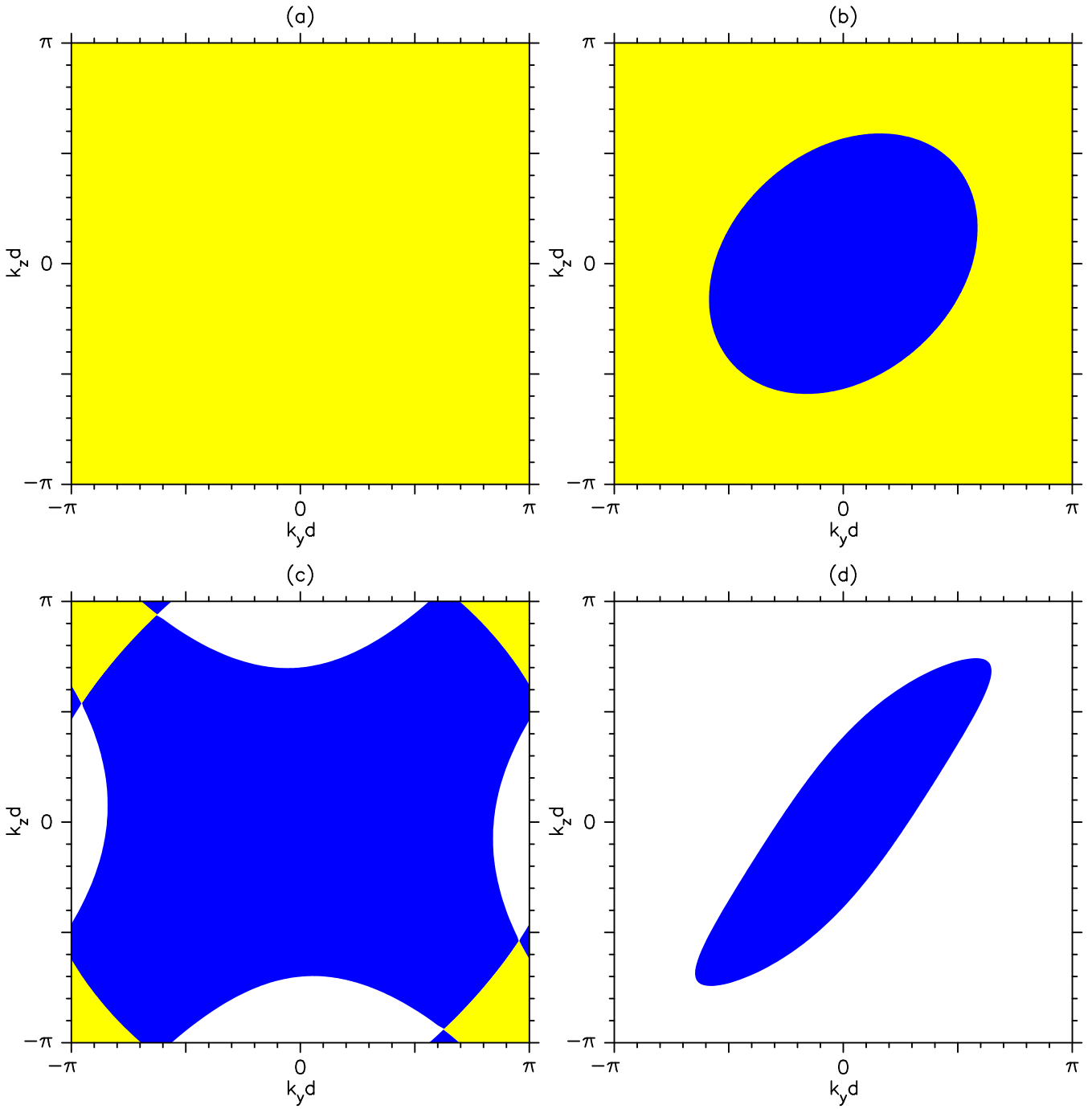

FIG. 4. (Color online) Examples of 2D flat bands with different phases in the 3D case. Yellow (light gray): a twofold degenerate zero-energy flat band. Blue (dark gray): a nondegenerate zero-energy flat band. White: no flat bands. (a) Phase 1: $J_{1,y} = J_{1,z} = 0.2$ and $J_{2,y} = J_{2,z} = 0.1$. (b) Phase 2: $J_{1,y} = 0.6$, $J_{1,z} = 0.4$, and $J_{2,y} = J_{2,z} = 0.2$. (c) Phase 3: $J_{1,y} = J_{1,z} = 1.0$, $J_{2,y} = 0.8$, and $J_{2,z} = 0.6$. (d) Phase 4: $J_{1,y} = 2.0$, $J_{1,z} = 1.2$, $J_{2,y} = 0.3$, and $J_{2,z} = 0.4$. (a)–(d) $J_{1,x} = 1.0$ and $J_{2,x} = 0.2$.

III. CONCLUSION

We have presented both 2D and 3D optical lattices, which possess topological surface flat bands. We have proven the unusual topological properties by two independent methods: an analytical calculation based on a topological winding number and numerical calculations of the eigenstates of the systems. These lattices can be relatively easily created by counterpropagating laser beams and do not require spin-orbit coupling or non-Abelian gauge fields. By tuning the intensity of the potential, it is possible to sweep between topological insulating, semimetallic, and trivial insulating phases.

The surface flat bands found here are protected by the particle-hole chiral symmetry given in Eq. (4), which requires the energy spectrum to be symmetric with respect to energy $E = 0$. In contrast to solid-state systems, optical lattices can be realized experimentally with high precision to follow this symmetry. Even in the case that a small particle-hole breaking

term is present in the Hamiltonian, the flat band is not destroyed, but is adiabatically deformed and becomes slightly dispersive [41,42].

We derived simple analytical formulas for the existence and the location of the flat bands. We showed that in the 3D case, we can have a double degeneracy of the flat bands. Also in the 3D case, the flat bands are two dimensional, in contrast to other surface flat band systems where the flat bands are one dimensional. Due to their short localization length, these flat bands could be realized in experiments even with a small lattice size.

These systems can be used to study the influence of interaction on the flat bands via a Feshbach resonance or to study high-T_c surface superfluidity. Also these systems can be used to model different flat band systems with little modification.

APPENDIX A: CREATION OF THE LATTICES

The corresponding 2D lattice can be formed using the following periodical potential:

$$V_{2D}(x,y) = V_1 \cos^2\left(\frac{2\pi x}{d}\right) + V_2 \cos^2\left(\frac{2\pi y}{d}\right) + V_3 \cos^2\left[\frac{\pi(x+y)}{d} + \theta_1\right] + V_4 \cos^2\left[\frac{\pi(x-y)}{d} + \theta_2\right]. \quad \text{(A1)}$$

To create this potential, we need four lasers with wavelength $\lambda_1 = d$ and four lasers with wavelength $\lambda_2 = \sqrt{2}d$, where d is the periodicity of the lattice. Figure 5 shows the laser arrangement schematically. We note that the four terms in Eq. (A1) should not interfere with each other. Experimentally, this can be accomplished by choosing the field directions perpendicular to each other or control of the relative time-phase delay [81]. Figure 6 shows an example of the 2D lattice potential. We can see from the figure that the barriers between the sublattice sites are different in the forward direction (alongside the axis) than in the backward direction. This means that the hopping strengths are different also. As regards the quality of the edges of the system, we note that sharp edges are not a critical requirement for the existence of topological surface states. The existence of the surface flat bands is topologically protected by the chiral symmetry given by Eq. (4). This symmetry remains valid also for smooth edges.

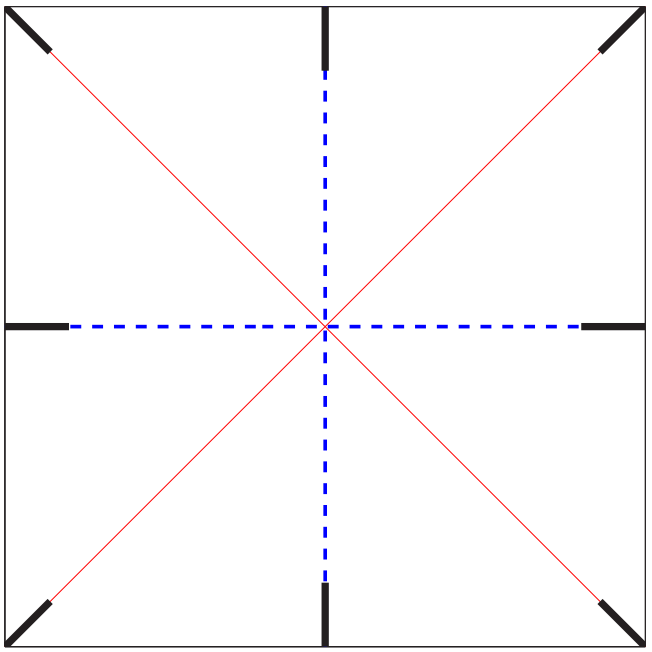

FIG. 5. (Color online) Schematic figure of the laser arrangement. Black sticks indicate the lasers, red solid lines indicate $\sqrt{2}\lambda$-laser beams, and blue dashed lines are λ-laser beams.

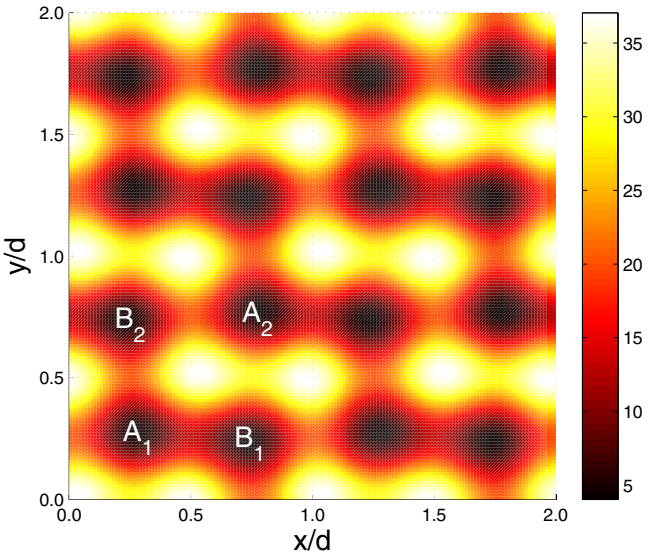

FIG. 6. (Color online) 2D lattice potential with $V_1 = 12E_r$, $V_2 = 20E_r$, $V_3 = 8E_r$, $V_4 = 1E_r$, $\theta_1 = \pi/4$, and $\theta_2 = -\pi/4$; $E_r = \hbar^2\pi^2/(md^2)$ is the recoil energy. White: high values; black: low values. The four lattice sites A_1, A_2, B_1, and B_2 from Fig. 1 are indicated in the first unit cell for comparison.

The three-dimensional lattice is a generalization of the 2D case. There are several ways to construct the three-dimensional potential. For the following potential, one needs 14 lasers, six with wavelength λ_1 and eight with λ_2. The potential is written as

$$V_{3D,1}(x,y,z) = V_1 \cos^2\left(\frac{2\pi x}{d}\right) + V_2 \cos^2\left(\frac{2\pi y}{d}\right) + V_3 \cos^2\left(\frac{2\pi z}{d}\right) + V_4 \cos^2\left[\frac{\pi(x+y)}{d} + \theta_1\right] + V_5 \cos^2\left[\frac{\pi(x-y)}{d} + \theta_2\right] + V_6 \cos^2\left[\frac{\pi(x+z)}{d} + \theta_3\right] + V_7 \cos^2\left[\frac{\pi(x-z)}{d} + \theta_4\right]. \quad \text{(A2)}$$

Alternatively, a more symmetric potential is given by

$$\begin{aligned} V_{3D,2}(x,y,z) = {} & V_1\cos^2\left(\frac{2\pi x}{d}\right) + V_2\cos^2\left(\frac{2\pi y}{d}\right) + V_3\cos^2\left(\frac{2\pi z}{d}\right) + V_4\cos^2\left[\frac{\pi(x+y)}{d} + \theta_1\right] \\ & + V_5\cos^2\left[\frac{\pi(x-y)}{d} + \theta_2\right] + V_6\cos^2\left[\frac{\pi(x+z)}{d} + \theta_3\right] + V_7\cos^2\left[\frac{\pi(x-z)}{d} + \theta_4\right] \\ & + V_8\cos^2\left[\frac{\pi(y+z)}{d} + \theta_5\right] + V_9\cos^2\left[\frac{\pi(y-z)}{d} + \theta_6\right]. \end{aligned} \tag{A3}$$

However, 18 lasers are needed to construct this potential.

APPENDIX B: SUPREMA AND INFIMA FOR THE 3D LATTICE

If $J_{1,x} \neq J_{2,x}$, then infima and suprema of $|V^+_{k_y,k_z}|$ and $|V^-_{k_y,k_z}|$ over the projected momentum space can be presented as functions of a_y, a_z, b_y, b_z. Without losing generality, we can assume $a_y, a_z, b_y, b_z \geqslant 0$. The supremum of $|V^+_{k_y,k_z}|$ is given by

$$\sup_{k_y,k_z}\left|V^+_{k_y,k_z}\right| = \begin{cases} a_y + a_z & \text{if} \quad a_y \geqslant b_y, a_z \geqslant b_z \\ b_y + b_z & \text{if} \quad a_y \leqslant b_y, a_z \leqslant b_z \\ \sqrt{\frac{\left(a_y^2 b_z^2 - a_z^2 b_y^2\right)\left(a_y^2 - b_y^2 + b_z^2 - a_z^2\right)}{\left(a_y^2 - b_y^2\right)\left(b_z^2 - a_z^2\right)}} & \text{if} \quad (a_y - b_y)(b_z - a_z) > 0; \quad x_0, y_0 \in \mathbb{R}; \quad \text{and} \quad |x_0|, |y_0| \leqslant 1 \\ \max(a_y + a_z, b_y + b_z) & \text{otherwise,} \end{cases} \tag{B1}$$

where

$$x_0 = \frac{b_y}{a_y^2 - b_y^2}\sqrt{\frac{-\left\{a_y^4 a_z^2 + a_z^2 b_y^4 - a_y^2\left[a_z^4 + b_z^4 + 2a_z^2\left(b_y^2 - b_z^2\right)\right]\right\}}{a_y^2 b_z^2 - a_z^2 b_y^2}},$$

$$y_0 = \frac{b_z}{b_z^2 - a_z^2}\sqrt{\frac{-\left\{a_y^4 a_z^2 + a_z^2 b_y^4 - a_y^2\left[a_z^4 + b_z^4 + 2a_z^2\left(b_y^2 - b_z^2\right)\right]\right\}}{a_y^2 b_z^2 - a_z^2 b_y^2}}.$$

The infimum of $|V^+_{k_y,k_z}|$ is given by

$$\inf_{k_y,k_z}\left|V^+_{k_y,k_z}\right| = \begin{cases} |b_y - b_z| & \text{if} \quad a_y \geqslant b_y, \quad a_z \geqslant b_z \\ a_y\sqrt{1 - \frac{b_z^2}{b_y^2 - a_y^2}} & \text{if} \quad a_y < b_y, \quad \frac{b_y b_z}{b_y^2 - a_y^2} \leqslant 1 \\ a_z\sqrt{1 - \frac{b_y^2}{b_z^2 - a_z^2}} & \text{if} \quad a_z < b_z, \quad \frac{b_y b_z}{b_z^2 - a_z^2} \leqslant 1 \\ |b_y - b_z| & \text{otherwise.} \end{cases} \tag{B2}$$

The supremum of $|V^-_{k_y,k_z}|$ is given by

$$\sup_{k_y,k_z}\left|V^-_{k_y,k_z}\right| = \begin{cases} \max\left(a_y, \sqrt{a_z^2 + b_y^2}\right) & \text{if} \quad b_z = 0 \\ \max\left(a_z, \sqrt{a_y^2 + b_z^2}\right) & \text{if} \quad b_y = 0 \\ b_y + b_z & \text{if} \quad a_y \leqslant b_y, a_z \leqslant b_z \\ a_y\sqrt{1 + \frac{b_z^2}{a_y^2 - b_y^2}} & \text{if} \quad a_y > b_y, \frac{b_y b_z}{a_y^2 - b_y^2} \leqslant 1 \quad \text{and} \quad a_z \leqslant b_z \text{ or } \frac{b_y b_z}{a_z^2 - b_z^2} > 1 \\ a_z\sqrt{1 + \frac{b_y^2}{a_z^2 - b_z^2}} & \text{if} \quad a_z > b_z, \frac{b_y b_z}{a_z^2 - b_z^2} \leqslant 1 \quad \text{and} \quad a_y \leqslant b_y \text{ or } \frac{b_y b_z}{a_y^2 - b_y^2} > 1 \\ \max\left(a_y\sqrt{1 + \frac{b_z^2}{a_y^2 - b_y^2}}, a_z\sqrt{1 + \frac{b_y^2}{a_z^2 - b_z^2}}\right) & \text{if} \quad a_z > b_y, a_z > b_z \quad \text{and} \quad \frac{b_y b_z}{a_y^2 - b_y^2} \leqslant 1, \frac{b_y b_z}{a_z^2 - b_z^2} \leqslant 1 \\ b_y + b_z & \text{otherwise.} \end{cases} \tag{B3}$$

The infimum of $|V^-_{k_y,k_z}|$ is given by

$$\inf_{k_y,k_z} |V^-_{k_y,k_z}| = \begin{cases} 0 & \text{if} \quad (a_y - a_z)(b_z - b_y) \geqslant 0 \\ \min(|a_y - a_z|, |b_y - b_z|) & \text{if} \quad (a_y - a_z)(b_z - b_y) < 0 \quad \text{and} \quad (a_y - b_y)(a_z - b_z) \leqslant 0 \\ \sqrt{\frac{\left(a_y^2 b_z^2 - a_z^2 b_y^2\right)\left(a_y^2 - b_y^2 + b_z^2 - a_z^2\right)}{\left(a_y^2 - b_y^2\right)\left(b_z^2 - a_z^2\right)}} & \text{if} \quad (a_y - b_y)(a_z - b_z) > 0; \quad x_1, y_1 \in \mathbb{R}; \quad \text{and} \quad |x_1|, |y_1| \leqslant 1 \\ \min(|a_y - a_z|, \quad |b_y - b_z|) & \text{otherwise,} \end{cases} \tag{B4}$$

where

$$x_1 = \frac{b_y}{a_y^2 - b_y^2} \sqrt{\frac{-\left\{a_y^4 a_z^2 + a_z^2 b_y^4 - a_y^2\left[a_z^4 + b_z^4 + 2a_z^2\left(b_y^2 - b_z^2\right)\right]\right\}}{a_y^2 b_z^2 - a_z^2 b_y^2}}$$

$$y_1 = \frac{b_z}{a_z^2 - b_z^2} \sqrt{\frac{-\left\{a_y^4 a_z^2 + a_z^2 b_y^4 - a_y^2\left[a_z^4 + b_z^4 + 2a_z^2\left(b_y^2 - b_z^2\right)\right]\right\}}{a_y^2 b_z^2 - a_z^2 b_y^2}}.$$

[1] B. A. Bernevig, T. L. Hughes, and S.-C. Zhang, Science **314**, 1757 (2006).
[2] L. Fu, C. L. Kane, and E. J. Mele, Phys. Rev. Lett. **98**, 106803 (2007).
[3] M. König, S. Wiedmann, C. Brüne, A. Roth, H. Buhmann, L. W. Molenkamp, X.-L. Qi, and S.-C. Zhang, Science **318**, 766 (2007).
[4] D. Hsieh, D. Qian, L. Wray, Y. Xia, Y. Hor, R. J. Cava, and M. Z. Hasan, Nature (London) **452**, 970 (2008).
[5] M. Z. Hasan and C. L. Kane, Rev. Mod. Phys. **82**, 3045 (2010).
[6] X. Wan, A. M. Turner, A. Vishwanath, and S. Y. Savrasov, Phys. Rev. B **83**, 205101 (2011).
[7] A. A. Burkov and L. Balents, Phys. Rev. Lett. **107**, 127205 (2011).
[8] Z. K. Liu *et al.*, Science **343**, 864 (2014).
[9] S. Borisenko, Q. Gibson, D. Evtushinsky, V. Zabolotnyy, B. Büchner, and R. J. Cava, Phys. Rev. Lett. **113**, 027603 (2014).
[10] S. Jeon, B. B. Zhou, A. Gyenis, B. E. Feldman, I. Kimchi, A. C. Potter, Q. D. Gibson, R. J. Cava, A. Vishwanath, and A. Yazdani, Nat. Mater. **13**, 851 (2014).
[11] Y. Yamaji and M. Imada, Phys. Rev. X **4**, 021035 (2014).
[12] K. I. Petsas, A. B. Coates, and G. Grynberg, Phys. Rev. A **50**, 5173 (1994).
[13] C. Orzel, A. K. Tuchman, M. L. Fenselau, M. Yasuda, and M. A. Kasevich, Science **291**, 2386 (2001).
[14] J. K. Chin, D. E. Miller, Y. Liu, C. Stan, W. Setiawan, C. Sanner, K. Xu, and W. Ketterle, Nature (London) **443**, 961 (2006).
[15] P. Windpassinger and K. Sengstock, Rep. Prog. Phys. **76**, 086401 (2013).
[16] C. Chin, R. Grimm, P. Julienne, and E. Tiesinga, Rev. Mod. Phys. **82**, 1225 (2010).
[17] M. Bartenstein, A. Altmeyer, S. Riedl, R. Geursen, S. Jochim, C. Chin, J. H. Denschlag, R. Grimm, A. Simoni, E. Tiesinga, C. J. Williams, and P. S. Julienne, Phys. Rev. Lett. **94**, 103201 (2005).
[18] T. D. Stanescu, V. Galitski, and S. Das Sarma, Phys. Rev. A **82**, 013608 (2010).
[19] K. Sun, W. V. Liu, A. Hemmerich, and S. Das Sarma, Nat. Phys. **8**, 67 (2012).
[20] Z. Lan, N. Goldman, A. Bermudez, W. Lu, and P. Öhberg, Phys. Rev. B **84**, 165115 (2011).
[21] M. Buchhold, D. Cocks, and W. Hofstetter, Phys. Rev. A **85**, 063614 (2012).
[22] F. Mei, S.-L. Zhu, Z.-M. Zhang, C. H. Oh, and N. Goldman, Phys. Rev. A **85**, 013638 (2012).
[23] J. Klinovaja and D. Loss, Phys. Rev. Lett. **111**, 196401 (2013).
[24] C. J. Kennedy, G. A. Siviloglou, H. Miyake, W. C. Burton, and W. Ketterle, Phys. Rev. Lett. **111**, 225301 (2013).
[25] F. Grusdt, D. Abanin, and E. Demler, Phys. Rev. A **89**, 043621 (2014).
[26] M. Atala, M. Aidelsburger, J. T. Barreiro, D. Abanin, T. Kitagawa, E. Demler, and I. Bloch, Nat. Phys. **9**, 795 (2013).
[27] G. Jotzu, M. Messer, R. Desbuquois, M. Lebrat, T. Uehlinger, D. Greif, and T. Esslinger, Nature (London) **515**, 237 (2014).
[28] M. Aidelsburger, M. Lohse, C. Schweizer, M. Atala, J. T. Barreiro, S. Nascimbène, N. R. Cooper, I. Bloch, and N. Goldman, Nat. Phys. **11**, 162 (2015).
[29] C. Wu, D. Bergman, L. Balents, and S. Das Sarma, Phys. Rev. Lett. **99**, 070401 (2007).
[30] C. Weeks and M. Franz, Phys. Rev. B **85**, 041104 (2012).
[31] K. Sun, Z. Gu, H. Katsura, and S. Das Sarma, Phys. Rev. Lett. **106**, 236803 (2011).
[32] O. V. Yazyev, Rep. Prog. Phys. **73**, 056501 (2010).
[33] N. B. Kopnin, JETP Lett. **94**, 81 (2011).
[34] N. B. Kopnin, M. Ijäs, A. Harju, and T. T. Heikkilä, Phys. Rev. B **87**, 140503(R) (2013).
[35] D. Bercioux, D. F. Urban, H. Grabert, and W. Häusler, Phys. Rev. A **80**, 063603 (2009).
[36] V. Apaja, M. Hyrkäs, and M. Manninen, Phys. Rev. A **82**, 041402(R) (2010).
[37] D. Guzman-Silva, C. Mejia-Cortes, M. A. Bandres, M. C. Rechtsman, S. Weimann, S. Nolte, M. Segev, A. Szameit, and R. A. Vicencio, New J. Phys. **16**, 063061 (2014).
[38] G.-W. Chern, C.-C. Chien, and M. Di Ventra, Phys. Rev. A **90**, 013609 (2014).
[39] S. Ryu and Y. Hatsugai, Phys. Rev. Lett. **89**, 077002 (2002).
[40] S. Matsuura, P.-Y. Chang, A. P. Schnyder, and S. Ryu, New J. Phys. **15**, 065001 (2013).
[41] T. Paananen and T. Dahm, Phys. Rev. B **87**, 195447 (2013).
[42] T. Paananen, H. Gerber, M. Götte, and T. Dahm, New J. Phys. **16**, 033019 (2014).

[43] K. Nakada, M. Fujita, G. Dresselhaus, and M. S. Dresselhaus, Phys. Rev. B **54**, 17954 (1996).
[44] T. Mizushima, M. Sato, and K. Machida, Phys. Rev. Lett. **109**, 165301 (2012).
[45] M. A. Silaev and G. E. Volovik, Phys. Rev. B **86**, 214511 (2012).
[46] A. P. Schnyder, C. Timm, and P. M. R. Brydon, Phys. Rev. Lett. **111**, 077001 (2013).
[47] P. M. R. Brydon, C. Timm, and A. P. Schnyder, New J. Phys. **15**, 045019 (2013).
[48] C. L. M. Wong, J. Liu, K. T. Law, and P. A. Lee, Phys. Rev. B **88**, 060504 (2013).
[49] J. D. Sau and S. Tewari, Phys. Rev. B **86**, 104509 (2012).
[50] A. Lau and C. Timm, Phys. Rev. B **88**, 165402 (2013).
[51] C.-R. Hu, Phys. Rev. Lett. **72**, 1526 (1994).
[52] Y. Tanaka and S. Kashiwaya, Phys. Rev. Lett. **74**, 3451 (1995).
[53] S. Kashiwaya and Y. Tanaka, Rep. Prog. Phys. **63**, 1641 (2000).
[54] G. E. Volovik, JETP Lett. **93**, 66 (2011).
[55] M. Sato, Y. Tanaka, K. Yada, and T. Yokoyama, Phys. Rev. B **83**, 224511 (2011).
[56] Y. Tanaka, M. Sato, and N. Nagaosa, J. Phys. Soc. Jpn. **81**, 011013 (2012).
[57] T. T. Heikkilä, N. B. Kopnin, and G. E. Volovik, JETP Lett. **94**, 233 (2011); G. E. Volovik, J. Supercond. Nov. Magn. **26**, 2887 (2013).
[58] F. F. Assaad, M. Bercx, and M. Hohenadler, Phys. Rev. X **3**, 011015 (2013).
[59] B. Roy, F. F. Assaad, and I. F. Herbut, Phys. Rev. X **4**, 021042 (2014).
[60] M. Götte, T. Paananen, G. Reiss, and T. Dahm, Phys. Rev. Appl. **2**, 054010 (2014).
[61] M. Sato, Phys. Rev. B **73**, 214502 (2006).
[62] M. Fogelström, D. Rainer, and J. A. Sauls, Phys. Rev. Lett. **79**, 281 (1997).
[63] H. Walter, W. Prusseit, R. Semerad, H. Kinder, W. Assmann, H. Huber, H. Burkhardt, D. Rainer, and J. A. Sauls, Phys. Rev. Lett. **80**, 3598 (1998).
[64] M. Aprili, E. Badica, and L. H. Greene, Phys. Rev. Lett. **83**, 4630 (1999).
[65] R. Krupke and G. Deutscher, Phys. Rev. Lett. **83**, 4634 (1999).
[66] C. Iniotakis, S. Graser, T. Dahm, and N. Schopohl, Phys. Rev. B **71**, 214508 (2005); K. W. Schmid, T. Dahm, J. Margueron, and H. Müther, *ibid.* **72**, 085116 (2005).
[67] B. Chesca, M. Seifried, T. Dahm, N. Schopohl, D. Koelle, R. Kleiner, and A. Tsukada, Phys. Rev. B **71**, 104504 (2005).
[68] B. Chesca, D. Doenitz, T. Dahm, R. P. Huebener, D. Koelle, R. Kleiner, Ariando, H.-J. H. Smilde, and H. Hilgenkamp, Phys. Rev. B **73**, 014529 (2006).
[69] C. Iniotakis, T. Dahm, and N. Schopohl, Phys. Rev. Lett. **100**, 037002 (2008).
[70] S. Graser, C. Iniotakis, T. Dahm, and N. Schopohl, Phys. Rev. Lett. **93**, 247001 (2004).
[71] A. Zare, T. Dahm, and N. Schopohl, Phys. Rev. Lett. **104**, 237001 (2010); A. Zare, A. Markowsky, T. Dahm, and N. Schopohl, Phys. Rev. B **78**, 104524 (2008).
[72] A. P. Zhuravel, B. G. Ghamsari, C. Kurter, P. Jung, S. Remillard, J. Abrahams, A. V. Lukashenko, A. V. Ustinov, and S. M. Anlage, Phys. Rev. Lett. **110**, 087002 (2013).
[73] T. Dahm and D. J. Scalapino, New J. Phys. **16**, 023003 (2014).
[74] D. A. Abanin, T. Kitagawa, I. Bloch, and E. Demler, Phys. Rev. Lett. **110**, 165304 (2013).
[75] K. Osterloh, M. Baig, L. Santos, P. Zoller, and M. Lewenstein, Phys. Rev. Lett. **95**, 010403 (2005).
[76] J. Ruseckas, G. Juzeliunas, P. Öhberg, and M. Fleischhauer, Phys. Rev. Lett. **95**, 010404 (2005).
[77] J. Zak, Phys. Rev. Lett. **62**, 2747 (1989).
[78] S. Ryu, A. P. Schnyder, A. Furusaki, and A. Ludwig, New J. Phys. **12**, 065010 (2010).
[79] A. P. Schnyder, S. Ryu, A. Furusaki, and A. W. W. Ludwig, Phys. Rev. B **78**, 195125 (2008).
[80] A. P. Schnyder and S. Ryu, Phys. Rev. B **84**, 060504(R) (2011); P. M. R. Brydon, A. P. Schnyder, and C. Timm, *ibid.* **84**, 020501(R) (2011); A. P. Schnyder, P. M. R. Brydon, and C. Timm, *ibid.* **85**, 024522 (2012).
[81] A. Hemmerich, D. Schropp, T. Esslinger, and T. W. Hänsch, Europhys. Lett. **18**, 391 (1992).